ACS APPLIED MATERIALS & INTERFACES

Research Article

www.acsami.org

Influence of Wetting on Morphology and Core Content in Electrospun Core–Sheath Fibers

Dae Kyom Kim[†] and Jan P. F. Lagerwall*[,†,‡]

[†]Graduate School of Convergence Science and Technology, Department of Nanoscience and Technology, Seoul National University, Suwon-si, Gyeonggi-do, Korea 443-270

[‡]Physics and Materials Science Research Unit, University of Luxembourg, Luxembourg, L-1523

Supporting Information

ABSTRACT: Coaxial electrospinning allows easy and cost-effective realization of composite fibers at the nano- and microscales. Different multifunctional materials can be incorporated with distinct localization to specific regimes of the fiber cross section and extended internal interfaces. However, the final composite properties are affected by variations in internal structure, morphology, and material separation, and thus, nanoscale control is mandatory for high-performance application in devices. Here, we present an analysis with unprecedented detail of the cross section of liquid core-functionalized fibers, yielding information that is difficult to reveal. This is based on focused ion beam (FIB) lift-out and allowing HR-TEM imaging of the fibers together with nanoscale resolution chemical analysis using energy dispersive X-ray spectroscopy (EDS). Unexpectedly, core material escapes during spinning and ends up coating the fiber exterior and target substrate. For high core injection rate, a dramatic difference in fiber morphology is found, depending on whether the surface on which the fibers are deposited is hydrophobic or hydrophilic. The latter enhances postspinning extraction of core fluid, resulting in the loss of the functional material and collapsed fiber morphology. Finally, in situ produced TiO_2 nanoparticles dispersed in the polymer appear strikingly different when the core fluid is present compared to when the polymer solution is spun on its own.

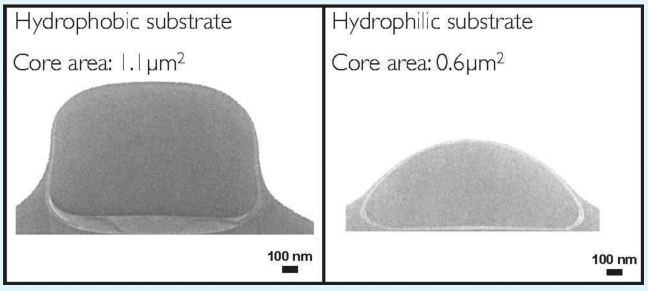

KEYWORDS: *electrospinning, core–sheath fibers, focused ion beam lift-out, capillary deformation, wetting*

1. INTRODUCTION

The present-day focus on miniaturization, multifunctionality, and incorporation of devices in media that traditionally were passive, such as for wearable and other flexible technology,[1−6] places high demands on novel advanced materials development, most notably in the realm of smart materials. Particularly appealing are hybrid materials that simultaneously incorporate multiple functions and attributes (sometimes conflicting), such as conductivity, transparency, light emission, sensory response, actuation, mechanical strength, or different refractive indices. A recently introduced promising route to achieve such materials is to produce core–sheath fibers, either by drawing[7−9] or spinning, whereby the latter approach has most strongly been pursued using the electrospinning technique.[10−22] Electrospun fiber mats are porous and lightweight, they have large effective surface area due to a fiber diameter typically in the micrometer range or lower, and they can be produced with a host of different materials and with complex fiber cross section, often combining a carrier polymer with one or more functional components that endow the composite with multiple attractive properties. This makes them ideal candidates for many cases of smart materials development.[6,10,20−25]

An important modification is coaxial electrospinning,[26−29] which recenlty has emerged as a potent method to functionalize the fibers with useful additives that are not spinnable on their own. Examples are low molar mass liquid crystals,[10,30−36] liquid metals,[21] suspensions of magnetic nanoparticles,[20,37] phase change materials,[18,19] or even live cells.[25] The method also allows the production of micro- and nanofibers that are hollow, and thus tube-like,[27−29,38−41] as well as a compartmentalization of the fiber interior with different geometries.[19,39,41]

Many details of coaxial electrospinning are, however, highly complex, and our understanding of the process is still inadequate for reliable production of high-quality core–sheath fibers with controlled internal structure. This is especially true when functional liquids are to be encapsulated at high filling fraction, and when relatively large overall fiber diameter (~1−5 μm range) yet a thin sheath (~100 nm) is desired, for instance to obtain strongly responsive fiber mats with an easily detectable output.[10,35] The overall fiber morphology can be quite far from the intuitively expected cylindrical one, as recently demonstrated by Enz et al. using focused ion beam (FIB) to section coaxially electrospun liquid crystal-functionalized microfibers.[36] The study revealed a cylinder segment

Received: July 27, 2014
Accepted: August 29, 2014
Published: August 29, 2014

morphology and a core channel that varied in shape and size throughout the fibers. To create the insight required for reliable production of complex multifunctional core−sheath fibers in an attractive diameter range by electrospinning, new analysis strategies are called for that provide a richly detailed picture of the entire process, complete enough to elucidate the key problems hampering development.

Here, we introduce such a strategy and demonstrate its potential to advance our understanding of coaxial electrospinning by applying it to a model core−sheath system with a liquid silicone oil core inside a composite sheath of polyvinylpyrrolidone (PVP) and TiO_2 nanoparticles synthesized in situ following hydrolysis of titanium(IV) isopropoxide ($Ti(O^iPr)_4$).[42] We use FIB for sectioning the fibers and performing a lift-out procedure[43] that allows us to image the core−sheath fiber cross section with unprecedented detail by high-resolution transmission electron microscopy (HR-TEM). Moreover, location-specific chemical analysis by energy dispersive X-ray spectroscopy (EDS) enables us to distinguish the different materials in sheath, core as well as in the fiber surroundings. Combined with optical microscopy (OM) and scanning electron microscopy (SEM) imaging of the overall fiber mats, an exceptionally complete picture emerges. The novel information revealed by the study puts the spotlight on aspects of the coaxial electrospinning process that are frequently overlooked—in particular the role of water condensing from the air and the related importance of the nature of the substrate on which the fibers are spun—yet may have a critical impact on the quality and nanoscale morphology of the final material.

2. EXPERIMENTAL SECTION

2.1. Materials. The sheath polymer was PVP with M_w = 1 300 000 g mol^{-1} (Acros). $Ti(O^iPr)_4$ was added as TiO_2 precursor with acetic acid as catalyst (both Aldrich). Silicone oil (kinematic viscosity 1000 cSt at 25 °C, molar mass about 30 000 g mol^{-1}), chloroform and anhydrous ethanol were purchased from Aldrich. All materials were used without further purification. Fibers were deposited on Si wafers with a 300 nm top layer of TiO_2 (Namkang Hi-Tech), either pristine or with a hydrophobic surface treatment. The latter was produced following the procedure of reference;[44] a summary is in the Supporting Information. Solution viscosities were measured at 25 °C with a TA Instruments AR-G2 rheometer (60 mm diameter, 1° cone and plate geometry) and contact angles with a Phoenix 150 surface angle analyzer (sessile drop method).

2.2. Electrospinning. A solution of PVP (9.5 wt %), $Ti(O^iPr)_4$ (3.0 wt %), and acetic acid (2.3 wt %) in anhydrous ethanol was used as sheath fluid, yielding in situ synthesis of TiO_2 via hydrolysis of $Ti(O^iPr)_4$, following the method of Xia and co-workers.[27] The fraction of inorganic component was, however, considerably lower in our case, yielding a final composite sheath with only 9% TiO_2; the remaining 91% was organic PVP. The core fluid was a mixture of silicone oil in chloroform (2:1 w/w), with a shear viscosity about 60% higher than that of the sheath solution. The electrospinning setup has been described in detail in an earlier paper,[34] and it is summarized in the Supporting Information along with further technical details. For simultaneous fiber collection on different substrates, a pristine chip and a hydrophobized one (both 5 × 5 mm^2) were placed next to each other on a glass slide kept 5 mm above the grounded electrode. The collection time was 2−3 s.

2.3. Optical and Electron Microscopy. After spinning, the fibers were left in air for ∼24 h to ensure complete solvent evaporation. Overview images were obtained using an optical microscope (Nikon Eclipse LV100) in reflection mode and a Hitachi S 4800 field emission scanning electron microscope (FE-SEM). Prior to SEM investigation, the samples were coated with platinum (3 nm thickness). For HR-TEM investigation of fiber cross sections, thin slices were prepared from the platinum-coated samples using the FIB lift-out method[43] (see Supporting Information for details).

3. RESULTS

Four different fiber types were spun, one without distinct core phase and the others with a silicone oil−chloroform mixture pumped as core fluid at 0.25, 0.75, and 1.2 mL h^{-1}, respectively. For all fibers, the flow rate of the PVP solution (sheath phase in case of coaxial spinning) was maintained at 1.75 mL h^{-1}. Representative overviews of fibers on a hydrophobic silicon substrate are shown in Figure 1, confirming the expected

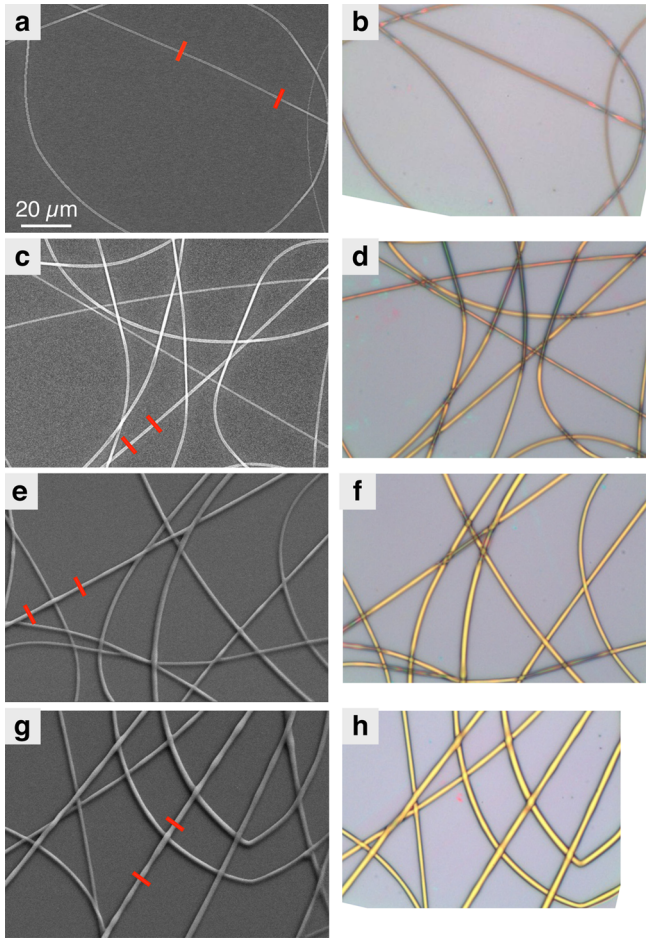

Figure 1. (a, c, e, and g) SEM and (b, d, f, and h) corresponding OM images of fiber samples collected on hydrophobic silicon substrates. The locations selected for FIB sectioning are indicated by red lines in the left panels. The fiber missing from panel a compared to panel b came off during transfer to the SEM chamber.

increase in fiber diameter with rising core flow rate. In no sample do we see merging of fibers at crossing points, demonstrating that the fiber exterior was no longer in a liquid state upon substrate impact. A slight tendency to beading is apparent from the 0.75 mL h^{-1} core flow rate and upward, indicating that the Rayleigh-Plateau instability is not fully suppressed at high core flow rate.

To gain a detailed view, we cut thin slices for HR-TEM imaging using the FIB lift-out technique at locations indicated in Figure 1, resulting in cross section images such as those in Figure 2 (images of other slices are shown in the Supporting Information). These images immediately reveal a number of

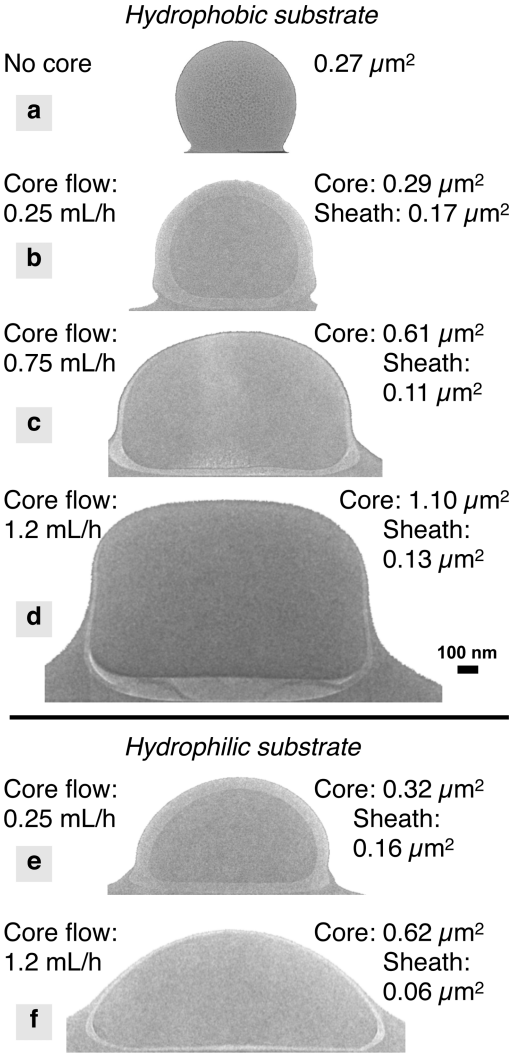

Figure 2. HR-TEM cross sections of fibers spun with varying core flow rate and deposited on (a–d) hydrophobic and (e–f) hydrophilic substrates. The respective sheath and core areas are indicated on the right. For clarity, the substrate and coating have been removed from the images (the raw images are in the Supporting Information).

interesting—and largely unexpected—details. First, the fiber cross section (with very well-defined core–sheath characteristics) does not only grow with increasing core flow rate, it also changes shape when the fibers are deposited on a hydrophobic substrate. While low filling leads to a fiber that is close to cylindrical, the strongly filled fibers have a cross section that is largely rectangular. This is in clear contrast to the fibers deposited on a hydrophilic substrate which generally have a horizontal cylinder segment morphology, similar to the fibers studied by Enz et al.[36] which were also deposited on hydrophilic substrates. Although the PVP sheath is not liquid after substrate impact (see above), it is obviously soft enough to adhere to and spread out along the hydrophilic surface in response to capillary forces, suggesting that the polymer is still swelled with solvent into a gel-like and easily deformable state.

A further important observation is that all fibers with silicone oil core are surrounded by a non-negligible amount of material outside the sheath. To establish its nature, we performed chemical analysis by EDS along selected scan directions through five different fibers at a total of 14 different locations. An example with two scans through the 0.25 mL h^{-1} core flow rate fiber deposited on hydrophobic substrate is shown in Figure 3. We recognize the sheath primarily through the strong

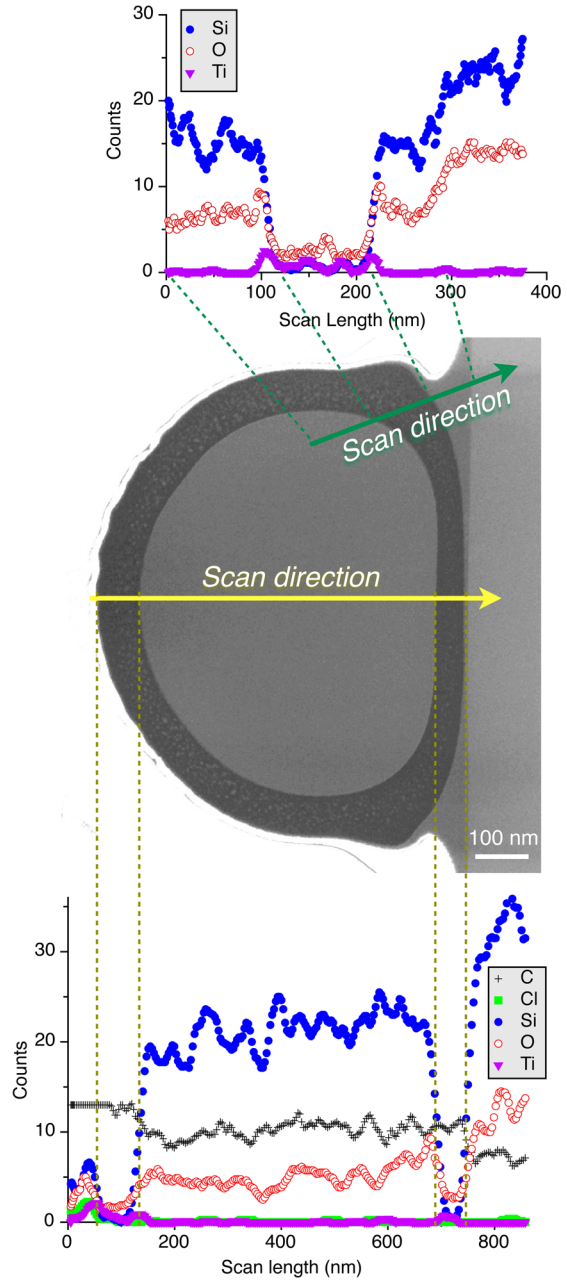

Figure 3. Location-specific chemical analysis by EDS through the 0.25 mL h^{-1} core flow rate fiber deposited on a hydrophobic substrate. Because of the weak strength of some signals, data have been smoothed over eight adjacent values for clarity.

dips in the Si and O signals. Their greater strength in the core region confirms that the silicone oil is well contained inside the fiber. The chloroform seems to have evaporated completely, as there is no Cl peak, except a small one on top of the fiber, possibly suggesting that a small fraction of titanium chloride formed during spinning.

We also notice local maxima outside the top sheath in the O and Si signals, giving a first hint that silicone oil has also escaped outside the sheath. This conclusion is corroborated in the zoomed-in scan shown at the top in Figure 3, which starts in the core and goes through the lower right-hand corner of the

fiber. The Si and O signals clearly reveal that the material outside the fibers, filling the space between substrate and sheath, is silicone oil (same intensities as in the fiber core, whereas the silicon oxide surface of the substrate yields distinctly stronger signals for both elements). Similar analysis for the other samples confirms that the material on the fiber outside is always silicone oil, for hydrophobic as well as hydrophilic substrates. In one case we used the FIB lift-out technique to also study a section along the fiber, as shown in Figure S5 (Supporting Information). Unfortunately, a partial collapse of the fiber top could not be prevented in this very fragile slice, but the data nevertheless prove that the core−sheath geometry is very uniform along the fiber. The consistent data from all slices studied (all transverse slices are shown in Figure S3, Supporting Information), as well as the stable trend as the core flow rate was varied, confirm that the data shown are representative for the fibers in general, supporting the generality of our conclusions.

The EDS analysis also quantitatively corroborates an interesting phenomenon that can be recognized qualitatively in the cross section images in Figure 2, namely that the TiO_2 nanoparticles interspersed in PVP are rather different in size and distribution in the single-phase fiber (Figure 2a) compared to the coaxial ones. While the inorganic component is barely noticeable in the sheaths of the coaxial fibers, many comparatively large clusters of TiO_2 are easy to spot in the center of the fiber without silicone oil core. The EDS scan through this fiber (Figure S6, Supporting Information) reveals a clear maximum of Ti signal around the fiber center, indicating larger and/or more numerous TiO_2 nanoparticles farther away from the fiber boundaries. This is surprising, considering recent reports based on in situ X-ray phase contrast imaging of the electrospinning process[45] and mechanical and optical measurements on electrospun conjugated polymer fibers by AFM/SNOM,[46] indicating that the polymer concentration in electrospun fibers should be greatest at the center. Such a situation should expel the TiO_2 nanoparticles toward the fiber perimeter.

The reported localization of polymer in the center was said to originate in the strong stretching of the polymer chains, reducing the lateral excursions of the polymer coils. We may thus speculate that the inorganic hydrolysis reaction in our experiment has a considerable effect on the polymer dynamics, counteracting stretching sufficiently to prevent the concentration of polymer to the core. Instead, a solid polymer skin forms on the outside due to rapid solvent evaporation, an effect observed experimentally and corroborated theoretically,[47,48] slowing further evaporation and promoting a solvent-enriched central region of the fiber. This also contains water condensed from the air (see below), enabling continued $Ti(O^iPr)_4$ hydrolysis. The extended liquid state allows nanoparticles forming at the jet center to aggregate and/or nucleate further growth into larger particles. In the thin sheath of the coaxial fibers, by contrast, the local variation in solvent content should be substantially lower. Moreover, the chloroform pushing through from the core, immiscible with water, should counteract absorption of condensed water into the sheath, thereby potentially restraining hydrolysis and the consequent TiO_2 particle formation process.

The areas of the core and sheath were measured graphically from the cross section images, as indicated numerically in Figure 2. Averages over the two slices investigated for each fiber type are plotted for the hydrophobic substrates in Figure 4. The

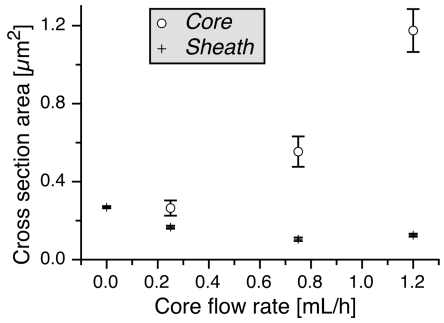

Figure 4. Cross section areas of the core and sheath of fibers deposited on hydrophobic silicon substrates as a function of core flow rate.

sheath area initially decreases with increasing core flow rate, although the sheath flow rate and the voltage that accelerates the jet during spinning were constant. This unexpected observation suggests that the fiber undergoes a greater degree of stretching the more core fluid is encapsulated. This is not unreasonable because the chloroform from the core fluid diffuses through the PVP sheath before it can evaporate. Because chloroform is a solvent for PVP, this prolongs the wet state of the sheath, and hence the more chloroform is delivered from the core, the greater the stretching. A further contribution should come from the reduced $Ti(O^iPr)_4$ hydrolysis, as discussed in the previous paragraph. Assuming volume conservation of PVP the stepwise reduction from 0.27 to 0.17 to 0.11 μm^2 as the core flow rate is increased from 0 to 0.75 mL h^{-1} would correspond to a roughly 35% increase in stretching for each step. The increased stretching must affect also the core when it is present, and indeed its area increases only by a factor of about 2 for the 3-fold increase in flow rate from 0.25 to 0.75 mL h^{-1}. This matches the behavior of the sheath very well.

At maximum core flow rate, this simple relation between stretching and cross section no longer holds. The sheath may now be so thin that further fiber stretching is inhibited, leading to the observed superlinear growth in core area in this region of the graph. As indicated by the larger error bar, the effect may also appear somewhat exaggerated, as an effect of the modulation of core cross section area that results from the increasingly important Rayleigh-Plateau instability (Figure 1 and related discussion). The sheath area even appears to increase somewhat at maximum core flow rate in Figure 4. However, this is likely to be an artifact due to the very low sheath thickness and the foam-like character of the polymer close to the hydrophobic substrate (Supporting Information), leading to systematic overestimates of the sheath area.

Going back to Figure 2, we note a further important difference between the fibers deposited on the two substrate types: the core area of fibers spun with high silicone oil flow rate and deposited on hydrophilic substrate is only about half that of the corresponding area of the same fiber deposited on a hydrophobic substrate. For both substrates, a second fiber slice was prepared by FIB lift-out and analyzed by HR-TEM (Supporting Information), corroborating the difference. Note that these fibers were all produced in the same experiment, and the two substrates were immediately next to each other while fibers were being deposited on them during steady-state spinning. The difference in fiber morphology must then be related to changes occurring in the fibers after deposition, not during spinning. The dramatic loss of silicone oil from the core

in the fiber depicted in Figure 2f, compared to the equivalent fiber in Figure 2d, must thus be a result of interaction with the substrate. This means that our findings are also relevant to the increasingly important field of near-field electrospinning,[6,49−52] in which all fibers are in direct contact with the substrate and deposited in a wet state due to the minimized solvent evaporation time frame in this technique. For multilayer mats produced by traditional spinning (including freely suspended mats), the substrate for the majority of the fibers will in fact be the previously deposited fibers. The same reasoning applies with the sheath polymer replacing the substrate material, albeit with additional complications due to the softness of the sheath and its consequent susceptiveness to be deformed by capillary forces. This means that the hydrophobicity or hydrophilicity of the fiber sheath should strongly influence the cross section and degree of filling of the composite fibers in the mat.

4. DISCUSSION

We will now conjecture a plausible model capable of explaining our observations. It is well-known that the cooling of the jet during electrospinning, resulting from the evaporation of the solvent, leads to condensation of water from the air. This event is fundamental for the hydrolysis of $Ti(O^iPr)_4$ into TiO_2,[42] and it can lead to a porous sheath.[53−55] In our coaxial experiments, this effect can be expected to be strong due to the rapidly evaporating chloroform. At the same time, the presence of this solvent should, as mentioned above, counteract the absorption of the condensed water into the jet, and we may thus assume that the fiber surface is surrounded by a thin layer of water (subject to capillary instabilities) when it lands on the substrate. If the latter is hydrophilic, then the water spreads, leaving the fiber such that silicone oil diffusing through the sheath from the core together with chloroform can spread as well (silicone oil spreads on all solid substrates considered in this work as well as on water[56]). Capillary forces between the spreading liquids and the sheath promote a flattening and spreading of the fiber along the substrate, as seen in Figure 2f. Moreover, as long as chloroform remains in the core, it will diffuse through the sheath (which is thus maintained in a wet gel-like state), allowing further silicone oil to escape with it. This explains the considerable depletion of core material seen in the fiber spun with high core injection and deposited on a hydrophilic substrate. With the lower core flow rate of 0.25 mL h^{-1} used for the fiber in Figure 2e, much less chloroform remains in the core at the time of deposition, leading to faster solidification of the sheath and a consequently reduced loss of core content and spreading of the fiber on the substrate. In the case of multilayer mats (free-hanging or deposited on a substrate), the fibers deposited after the bottom layer will experience the same phenomenon if the polymer sheath itself is hydrophilic, as is the case for PVP and other water-soluble polymers used for electrospinning. A further complication (beyond the scope of this paper) in this case is the absorption of the spreading water into the polymer, prolonging the soft state of the previously deposited fibers.

If the jet instead hits a hydrophobic substrate, then the water on its outside cannot spread but will form an asymmetric meniscus along the length of the fiber. Water has a contact angle of 104° on our hydrophobic substrate (Supporting Information), limiting the extension of the meniscus away from the fiber. The PVP-based fiber, by contrast, is wetted by water, allowing it to climb high on this preferred surface. First of all, this can explain the tendency toward a rectangular cross section of the fibers deposited on hydrophobic substrates, as the side of the sheath will experience capillary forces from both the inside and the outside, promoting a vertical orientation if the forces are balanced. Second, the water lining the fiber outside prevents chloroform and silicone oil to escape through the sheath along the sides, leaving only the top as a possible escape route. On the other hand, it is beneficial for hydrolysis of $Ti(O^iPr)_4$, resulting in a spatially varying TiO_2 concentration with local maxima along the sheath sides (see Figure 3). Because of the comparatively slow evaporation of water, which is further slowed due to the cooling by continued chloroform evaporation, the core will lose all its chloroform through the top of the sheath. By the time the water has left the fiber, the sheath has solidified, retaining the remaining silicone oil inside, and thus, much less core material is lost than in the fiber on the hydrophilic substrate. The amount of silicone oil that has nevertheless escaped will eventually have access to the substrate, leaving the final meniscus seen on the fiber outside in Figure 2. The temporary water meniscus has, however, left a trace in the form of an unusual deformation of the sheath. This is most clearly visible in Figure 2b, where the silicone oil meniscus is much smaller than the water meniscus that was present as the sheath solidified, pulling the sheath outward on both sides about 150 nm above the substrate.

It is important to note that the water solubility of the PVP sheath is not a prerequisite for these phenomena to occur, because the origin of water condensation is the cooling due to solvent evaporation. Even when we use sheath polymers that are insoluble in water, the fiber cooling leads to significant condensation of water. Once the fiber hits the substrate, essentially the same difference in postdeposition fiber modification can be expected, in particular regarding the loss of core content, depending on whether the substrate is hydrophilic or hydrophobic. In case the fiber sheath polymer itself is hydrophobic, a difference is that the water cannot climb up the side of the deposited fiber, and hence, the rectangular cross section seen in this work for strongly filled fibers on hydrophobic substrates would not be expected.

There are several reports of coaxially spun fibers with close to cylindrical cross section, such as the seminal work by Li and Xia.[27] However, these fibers are typically of very small diameter (well below 1 μm), and the sheath cross-sectional area is comparable to that of the core. In this range of modestly filled fibers with extremely small overall diameter, the cylindrical morphology can be maintained. This is in line with the trend observed in Figure 2. But when large diameter and thin sheath are desired, the fibers are strongly susceptible to deformation and collapse in response to capillary forces.[36,40]

While the presence of chloroform in the core fluid enhances these effects, the condensation of water on the fiber sheath also occurs for other core fluids because the evaporation of the sheath solvent cools the fiber. This leads to fiber spreading and flattening on hydrophilic substrates, as seen, for instance, in the study by Enz et al.[36] The possibility of pore formation in the sheath[53−55] will make loss of a liquid core to the outside a risk, even when no core solvent is used. For the case of solidifying polymeric cores, an escape is unlikely, but fiber flattening and deviation from cylindrical symmetry should then be considerable, as such core solutions typically contain a much higher fraction of evaporating solvent. Hence, hydrophobic substrates are greatly preferred when collecting electrospun core−sheath fibers with a thick core, and a hydrophobic sheath polymer will be of advantage if multilayer mats are spun.

5. CONCLUSION

Exceptionally detailed information about the nanoscale internal morphology of coaxially electrospun core−sheath fibers is provided by HR-TEM imaging and locally resolved chemical analysis by EDS on fiber cross-sectional slices prepared using the FIB lift-out method. Our key findings are that (1) even for a core material that is immiscible with the sheath solution, a non-negligible fraction escapes through the sheath and ends up on the fiber outside, in particular for fibers with large diameter and high degree of filling; (2) the deposition of such fibers on hydrophobic surfaces is highly advantageous, because hydrophilic surfaces are wetted by the water that condenses on the cold jet during spinning, inducing an outward liquid flow that depletes the fiber core and deforms the entire fiber after spinning; and (3) contrary to expectation, the polymer concentration is not the highest at the fiber center when in situ production of inorganic nanoparticles takes place during spinning, suggesting that the chemical reaction may influence the polymer chain dynamics such that stretching is reduced. The new data provide a much more complete picture of the coaxial electrospinning process and reveal for the first time the important role of hydrophilicity or hydrophobicity of the surfaces with which newly produced fibers come in contact. Together with the demonstration of the powerful combination of FIB, HR-TEM, and EDS, this gives a significant contribution to the ongoing efforts to realize increasingly advanced composite smart materials using electrospinning.

■ ASSOCIATED CONTENT

Ⓢ Supporting Information

Further HR-TEM and SEM images of fiber cross sections, additional EDS spectra, viscosity and contact angle data, extended descriptions of experimental procedures, and discussion of the unusual bottom sheath morphology seen at maximum core flow rate on hydrophobic substrates. This material is available free of charge via the Internet at http://pubs.acs.org.

■ AUTHOR INFORMATION

Corresponding Author

*E-mail: jan.lagerwall@lcsoftmatter.com.

Author Contributions

The manuscript was written through contributions of both authors. Both authors have given approval to the final version of the manuscript.

Notes

The authors declare no competing financial interest.

■ ACKNOWLEDGMENTS

We thank G. Scalia for valuable advice on FIB fiber sectioning and valuable comments on this manuscript. Moon Hee Park is thanked for assistance with FIB lift-out sample preparation, and Bo Seul Kim and Hae Na Yoo are thanked for assistance with TEM and EDS characterization. Financial support from the Seoul National University Foundation fund (Grant 490-20110040) and from Korea Advanced Nanofab Center (Grant K130725054) is gratefully acknowledged.

■ REFERENCES

(1) Lee, Y. H.; Kim, J. S.; Noh, J.; Lee, I.; Kim, H. J.; Choi, S.; Seo, J.; Jeon, S.; Kim, T. S.; Lee, J. Y.; Choi, J. W. Wearable Textile Battery Rechargeable by Solar Energy. *Nano Lett.* **2013**, *13*, 5753−5761.

(2) Wu, W.; Bai, S.; Yuan, M.; Qin, Y.; Wang, Z. L.; Jing, T. Lead Zirconate Titanate Nanowire Textile Nanogenerator for Wearable Energy-Harvesting and Self-Powered Devices. *ACS Nano* **2012**, *6*, 6231−6235.

(3) Kramer, R. K.; Majidi, C.; Wood, R. J. Wearable Tactile Keypad with Stretchable Artificial Skin. *IEEE Trans. Robot. Automat.* **2011**, 1103−1107.

(4) Cherenack, K.; Zysset, C.; Kinkeldei, T.; Munzenrieder, N.; Tröster, G. Woven Electronic Fibers with Sensing and Display Functions for Smart Textiles. *Adv. Mater.* **2010**, *22*, 5178−5182.

(5) Rogers, J. A.; Someya, T.; Huang, Y. Materials and Mechanics for Stretchable Electronics. *Science* **2010**, *327*, 1603−1607.

(6) Min, S.-Y.; Kim, T.-S.; Kim, B. J.; Cho, H.; Noh, Y.-Y.; Yang, H.; Cho, J. H.; Lee, T.-W. Large-Scale Organic Nanowire Lithography and Electronics. *Nat. Commun.* **2013**, *4*, 1773.

(7) Stolyarov, A. M.; Wei, L.; Shapira, O.; Sorin, F.; Chua, S. L.; Joannopoulos, J. D.; Fink, Y. Microfluidic Directional Emission Control of an Azimuthally Polarized Radial Fibre Laser. *Nat. Photonics* **2012**, *6*, 229−233.

(8) Stolyarov, A. M.; Wei, L.; Sorin, F.; Lestoquoy, G.; Joannopoulos, J. D.; Fink, Y. Fabrication and Characterization of Fibers with Built-In Liquid Crystal Channels and Electrodes for Transverse Incident-Light Modulation. *Appl. Phys. Lett.* **2012**, *101*, 011108.

(9) Abouraddy, A. F.; Bayindir, M.; Benoit, G.; Hart, S. D.; Kuriki, K.; Orf, N.; Shapira, O.; Sorin, F.; Temelkuran, B.; Fink, Y. Towards Multimaterial Multifunctional Fibres that See, Hear, Sense, and Communicate. *Nat. Mater.* **2007**, *6*, 336−347.

(10) Kim, D. K.; Hwang, M.; Lagerwall, J. P. F. Liquid Crystal-Functionalization of Electrospun Polymer Fibers. *J. Polym. Sci., Part B: Polym. Phys.* **2013**, *51*, 855−867.

(11) Cho, H.; Min, S.-Y.; Lee, T.-W. Electrospun Organic Nanofiber Electronics and Photonics. *Macromol. Mater. Eng.* **2013**, *298*, 475−486.

(12) Choi, S. H.; Youn, D. Y.; Jo, S. M.; Oh, S. G.; Kim, I. D. Micelle-Mediated Synthesis of Single-Crystalline β(3C)-SiC Fibers via Emulsion Electrospinning. *ACS Appl. Mater. Interfaces.* **2011**, *3*, 1385−1389.

(13) Lee, J. S.; Kwon, O. S.; Park, S. J.; Park, E. Y.; You, S. A.; Yoon, H.; Jang, J. Fabrication of Ultrafine Metal-Oxide-Decorated Carbon Nanofibers for DMMP Sensor Application. *ACS Nano* **2011**, *5*, 7992−8001.

(14) Krogman, K. C.; Lowery, J. L.; Zacharia, N. S.; Rutledge, G. C.; Hammond, P. T. Spraying Asymmetry into Functional Membranes Layer-by-Layer. *Nat. Mater.* **2009**, *8*, 512−518.

(15) Camposeo, A.; Di Benedetto, F.; Stabile, R.; Neves, A. A. R.; Cingolani, R.; Pisignano, D. Laser Emission from Electrospun Polymer Nanofibers. *Small* **2009**, *5*, 562−566.

(16) Agarwal, S.; Greiner, A.; Wendorff, J. H. Electrospinning of Manmade and Biopolymer Nanofibers—Progress in Techniques, Materials, and Applications. *Adv. Funct. Mater.* **2009**, *19*, 2863−2879.

(17) Kwak, G.; Lee, G. H.; Shim, S. H.; Yoon, K. B. Fabrication of Light-Guiding Core/Sheath Fibers By Coaxial Electrospinning. *Macromol. Rapid Commun.* **2008**, *29*, 815−820.

(18) McCann, J. T.; Marquez, M.; Xia, Y. N. Melt Coaxial Electrospinning: A Versatile Method for the Encapsulation of Solid Materials and Fabrication of Phase Change Nanofibers. *Nano Lett.* **2006**, *6*, 2868−2872.

(19) Wang, N.; Chen, H. Y.; Lin, L.; Zhao, Y.; Cao, X. Y.; Song, Y. L.; Jiang, L. Multicomponent Phase Change Microfibers Prepared by Temperature Control Multifluidic Electrospinning. *Macromol. Rapid Commun.* **2010**, *31*, 1622−1627.

(20) Medina-Castillo, A. L.; Fernández-Sánchez, J. F.; Fernández-Gutiérez, A. One-Step Fabrication of Multifunctional Core-Shell Fibres by Co-Electrospinning. *Adv. Funct. Mater.* **2011**, *21*, 3488−3495.

(21) Yang, H.; Lightner, C. R.; Dong, L. Light-Emitting Coaxial Nanofibers. *ACS Nano* **2012**, *6*, 622−628.

(22) Lee, K. J.; Yoon, J.; Rahmani, S.; Hwang, S.; Bhaskar, S.; Mitragotri, S.; Lahann, J. Spontaneous Shape Reconfigurations in

Multicompartmental Microcylinders. *Proc. Natl. Acad. Sci. U.S.A.* **2012**, *109*, 16057−16062.
(23) Park, M.; Im, J.; Shin, M.; Min, Y.; Park, J.; Cho, H.; Park, S.; Shim, M. B.; Jeon, S.; Chung, D. Y.; Bae, J.; Park, J.; Jeong, U.; Kim, K. Highly Stretchable Electric Circuits from a Composite Material of Silver Nanoparticles and Elastomeric Fibres. *Nat. Nanotechnol.* **2012**, *7*, 803−809.
(24) Park, J. H.; Braun, P. V. Coaxial Electrospinning of Self-Healing Coatings. *Adv. Mater.* **2009**, *22*, 496−499.
(25) Zussman, E. Encapsulation of Cells within Electrospun Fibers. *Polym. Adv. Technol.* **2011**, *22*, 366−371.
(26) Yarin, A. L. Coaxial Electrospinning and Emulsion Electrospinning of Core-Shell Fibers. *Polym. Adv. Technol.* **2011**, *22*, 310−317.
(27) Li, D.; Xia, Y. N. Direct Fabrication of Composite and Ceramic Hollow Nanofibers By Electrospinning. *Nano Lett.* **2004**, *4*, 933−938.
(28) Loscertales, I. G.; Barrero, A.; Marquez, M.; Spretz, R.; Velarde-Ortiz, R.; Larsen, G. Electrically Forced Coaxial Nanojets for One-Step Hollow Nanofiber Design. *J. Am. Chem. Soc.* **2004**, *126*, 5376−5377.
(29) McCann, J. T.; Li, D.; Xia, Y. N. Electrospinning of Nanofibers with Core-Sheath, Hollow, or Porous Structures. *J. Mater. Chem.* **2005**, *15*, 735−738.
(30) Buyuktanir, E. A.; Frey, M. W.; West, J. L. Self-Assembled, Optically Responsive Nematic Liquid Crystal/Polymer Core-Shell Fibers: Formation and Characterization. *Polymer* **2010**, *51*, 4823−4830.
(31) Enz, E.; Baumeister, U.; Lagerwall, J. Coaxial Electrospinning of Liquid Crystal-Containing Poly(vinyl pyrrolidone) Microfibers. *Beilstein J. Org. Chem.* **2009**, *5*, DOI: 10.3762/bjoc.5.58.
(32) Lagerwall, J. P. F.; McCann, J. T.; Formo, E.; Scalia, G.; Xia, Y. Coaxial Electrospinning of Microfibres With Liquid Crystal in the Core. *Chem. Commun.* **2008**, *42*, 5420−5422.
(33) Scalia, G.; Enz, E.; Calò, O.; Kim, D. K.; Hwang, M.; Lee, J. H.; Lagerwall, J. P. F. Morphology and Core Continuity of Liquid-Crystal-Functionalized, Coaxially Electrospun Fiber Mats Tuned via the Polymer Sheath Solution. *Macromol. Mater. Eng.* **2013**, *298*, 583−589.
(34) Liang, H.-L.; Enz, E.; Scalia, G.; Lagerwall, J. Liquid Crystals in Novel Geometries Prepared by Microfluidics and Electrospinning. *Mol. Cryst. Liq. Cryst.* **2011**, *549*, 69−77.
(35) Enz, E.; Lagerwall, J. Electrospun Microfibres with Temperature Sensitive Iridescence from Encapsulated Cholesteric Liquid Crystal. *J. Mater. Chem.* **2010**, *20*, 6866−6872.
(36) Enz, E.; La Ferrara, V.; Scalia, G. Confinement-Sensitive Optical Response of Cholesteric Liquid Crystals in Electrospun Fibers. *ACS Nano* **2013**, *7*, 6627−6635.
(37) Sharma, N.; Jaffari, G. H.; Shah, S. I.; Pochan, D. J. Orientation-Dependent Magnetic Behavior in Aligned Nanoparticle Arrays Constructed by Coaxial Electrospinning. *Nanotechnology* **2010**, *21*, 85707.
(38) Chan, K. H. K.; Kotaki, M. Fabrication and Morphology Control of Poly(methyl methacrylate) Hollow Structures via Coaxial Electrospinning. *J. Appl. Polym. Sci.* **2008**, *111*, 408−416.
(39) Zhao, Y.; Cao, X. Y.; Jiang, L. Bio-Mimic Multichannel Microtubes by a Facile Method. *J. Am. Chem. Soc.* **2007**, *129*, 764−765.
(40) Dror, Y.; Salalha, W.; Avrahami, R.; Zussman, E.; Yarin, A. L.; Dersch, R.; Greiner, A.; Wendorff, J. H. One-Step Production of Polymeric Microtubes by Co-Electrospinning. *Small* **2007**, *3*, 1064−1073.
(41) Chen, H. Y.; Wang, N.; Di, J. C.; Zhao, Y.; Song, Y. L.; Jiang, L. Nanowire-in-Microtube Structured Core/Shell Fibers via Multifluidic Coaxial Electrospinning. *Langmuir* **2010**, *26*, 11291−11296.
(42) Li, D.; Xia, Y. N. Fabrication of Titania Nanofibers by Electrospinning. *Nano Lett.* **2003**, *3*, 555−560.
(43) Giannuzzi, L. A.; Drown, J. L.; Brown, S. R.; Irwin, R. B.; Stevie, F. A. Applications of the FIB Lift-Out Technique for TEM Specimen Preparation. *Microsc. Res. Technol.* **1998**, *41*, 285−290.
(44) Kim, S. H.; Cui, Y.; Lee, M. J.; Nam, S. W.; Oh, D.; Kang, S. H.; Kim, Y. S.; Park, S. Simple Fabrication of Hydrophilic Nanochannels Using the Chemical Bonding between Activated Ultrathin PDMS Layer and Cover Glass by Oxygen Plasma. *Lab Chip* **2011**, *11*, 348−353.
(45) Greenfeld, I.; Fezzaa, K.; Rafailovich, M. H.; Zussman, E. Fast X-ray Phase-Contrast Imaging of Electrospinning Polymer Jets: Measurements of Radius, Velocity, and Concentration. *Macromolecules* **2012**, *45*, 3616−3626.
(46) Camposeo, A.; Greenfeld, I.; Tantussi, F.; Pagliara, S.; Moffa, M.; Fuso, F.; Allegrini, M.; Zussman, E.; Pisignano, D. Local Mechanical Properties of Electrospun Fibers Correlate to their Internal Nanostructure. *Nano Lett.* **2013**, *13*, 5056−5062.
(47) Arinstein, A.; Zussman, E. Electrospun Polymer Nanofibers: Mechanical and Thermodynamic Perspectives. *J. Polym. Sci., Part B: Polym. Phys.* **2011**, *49*, 691−707.
(48) Guenthner, A. J.; Khombhongse, S.; Liu, W.; Dayal, P.; Reneker, D. H.; Kyu, T. Dynamics of Hollow Nanofiber Formation During Solidification Subjected to Solvent Evaporation. *Macromol. Theory Simul.* **2006**, *15*, 87−93.
(49) Bisht, G. S.; Canton, G.; Mirsepassi, A.; Kuinsky, L.; Oh, S.; Dunn-Rankin, D.; Madou, M. J. Controlled Continuous Patterning of Polymeric Nanofibers on Three-Dimensional Substrates Using Low-Voltage Near-Field Electrospinning. *Nano Lett.* **2011**, *11*, 1831−1837.
(50) Chang, C.; Tran, V. H.; Wang, J.; Fuh, Y. K.; Lin, L. Direct-Write Piezoelectric Polymeric Nanogenerator with High Energy Conversion Efficiency. *Nano Lett.* **2010**, *10*, 726−731.
(51) Chang, C.; Limkrailassiri, K.; Lin, L. W. Continuous Near-Field Electrospinning for Large Area Deposition of Orderly Nanofiber Patterns. *Appl. Phys. Lett.* **2008**, *93*, 123111.
(52) Sun, D. H.; Chang, C.; Li, S.; Lin, L. W. Near-Field Electrospinning. *Nano Lett.* **2006**, *6*, 839−842.
(53) Lu, P.; Xia, Y. Maneuvering the Internal Porosity and Surface Morphology of Electrospun Polystyrene Yarns by Controlling the Solvent and Relative Humidity. *Langmuir* **2013**, *29*, 7070−7078.
(54) Casper, C. L.; Stephens, J. S.; Tassi, N. G.; Chase, D. B.; Rabolt, J. F. Controlling Surface Morphology of Electrospun Polystyrene Fibers: Effect of Humidity and Molecular Weight in the Electrospinning Process. *Macromolecules* **2004**, *37*, 573−578.
(55) Megelski, S.; Stephens, J. S.; Chase, D. B.; Rabolt, J. F. Micro- and Nanostructured Surface Morphology on Electrospun Polymer Fibers. *Macromolecules* **2002**, *35*, 8456−8466.
(56) de Gennes, P.-G.; Brochard-Wyart, F.; Quere, D. *Capillarity and Wetting Phenomena: Drops, Bubbles, Pearls, Waves*, trans. Axel Reisinger. Springer: New York, 2004.